Lab on a Chip

Room-temperature bonding of glass chips via PTFE-assisted plasma modification for nanofluidic applications

Journal:	*Lab on a Chip*
Manuscript ID	LC-COM-02-2023-000169.R1
Article Type:	Communication
Date Submitted by the Author:	07-May-2023
Complete List of Authors:	Kang, Qiushi; Harbin Institute of Technology State Key Laboratory of Advanced Welding and Joining Wang, Chenxi; Harbin Institute of Technology, State Key Laboratory of Advanced Welding and Joining Liu, Kaimeng; Harbin Institute of Technology State Key Laboratory of Advanced Welding and Joining Kitamori, Takehiko; The University of Tokyo

Room-temperature bonding of glass chips via PTFE-assisted plasma modification for nanofluidic applications

Qiushi Kang[a], Chenxi Wang [a]*, Kaimeng Liu[a], Takehiko Kitamori[b]

[a] State Key Laboratory of Advanced Welding and Joining, Harbin Institute of Technology, Harbin 150001, China. Email: wangchenxi@hit.edu.cn

[b] Collaborative Research Organization for Micro and Nano Multifunctional Devices, The University of Tokyo, 7-3-1 Hongo, Bunkyo, Tokyo 113-8656, Japan.

*Corresponding author: wangchenxi@hit.edu.cn

Abstract: Fused-silica glass, as a desirable material with rigidity, biological inertness, and favorable light transmission for nanofluidic devices, should be assembled via low-temperature bonding technology to hermetically seal channels for stable liquid manipulation in extended-nano ($10^1 \sim 10^3$ nm) space. Confronted with the predicament of localized functionalization of nanofluidic applications (e.g. DNA microarray) with temperature-sensitive structures, the room-temperature direct bonding of glass chips to achieve modification of channels prior to bonding offers a considerably attractive solution to avoid components denaturation during the conventional post-bonding heating process. Therefore, we developed a nano-structure friendly and technically convenient room-temperature (RT, 25 ℃) glass-glass direct bonding technology using polytetrafluoroethylene (PTFE)-assisted plasma modification without the requirement for special equipment. Unlike the establishment of chemical functionalities relying on immersion in potent but dangerous chemicals like HF, the fluorine radicals (F*) from PTFE pieces with superior chemical inertness were introduced on the glass surfaces via O_2 plasma sputtering and constructed fluorinated silicon oxides on the glass surfaces effectively, eliminating the significant etching effect of HF to protect fine nanostructures. Very strong bonding was obtained at RT with no heating and the high-pressure resistant glass-glass interfaces were evaluated under high-pressure-driven flow conditions up to 2 MPa based on a two-channel liquid introduction system. Moreover, the favorable optical transmittance of the fluorinated bonding interface demonstrated the capacity for high-resolution optical detection or liquid sensing.

Keywords: Glass, bonding, room temperature, PTFE, non-leakage, transmittance

1. Introduction

The concept of lab-on-a-chip aims to integrate the capability of a laboratory into a miniaturized nanofluidic system for rapid and accurate detection at the chip scale which is close to commercial reality. Owing to the manipulation of liquid-containing reagents with extended-nano scale (typically $10^1 \sim 10^3$ nm) to control reactions, nanofluidics has attracted many concerns for their promising applications using its dominant surface effect and extremely small volume, spanning disease monitoring and management, chemical synthesis, biomedical tissue engineering, and environmental sampling [1-5]. Compared with well-established polymer substrates (e.g. polydimethylsiloxane, PDMS) with low stiffness and water permeability, fused-silica glass substrates are extensively used for nanofluidic devices because they offer overwhelming advantages including chemical inertness, higher values of Young's modulus and light transmission, which can fabricate nanostructures with high resolution and avoid fluid leaching and evaporation [6, 7]. To achieve nanofluidic devices successfully, it is paramount to construct and hermetically seal channels via assembling glass substrates with nanostructures. To date, low-temperature bonding provides a desirable assemble solution with the merits of protecting high-temperature sensitive functional components immobilized in the channels such as biomolecules, electrodes, sensors, waveguides, optical components, etc [8]. Adhesive bonding (intermediate-layer bonding), as an important bonding technology performed at low temperatures, can integrate polymer, semiconductor, metal, and ceramic substrates by introducing micron-thick thermal or photo curable resin at the interface. The seamless, void-free robust glass bonding interface has been obtained through PDMS [9, 10], SU-8 [11], benzocyclobutene (BCB) [12, 13] within 300 °C. However, the dispensing of adhesive resin poses the potential for channel contamination and clogging, and adhesive bonds are not stable enough for long-term service due to the chemical reactivity of resins.

As a clogging-free solution for nanofluidic applications, a direct bonding approach flourishes relying on the low-temperature chemical reactions between the functionalized surface to achieve covalent bonds eventually, also known as "chemical gluing" [14]. Rather than the use of micron-scale resins, the liquid chemical "glue" (e.g., 3-aminopropyl trimethoxysilane, APTES) as crosslinking agents can establish nanometer-scale self-assembled monolayer (SAM) on the surface through several-hours immersion, reducing the risk of channel clogging and interfacial instability [15, 16]. It is reported that the C-C or Si-O-Si bonds can be achieved at 150~200 °C between the hydroxylated, aminosilylated, or carboxylated glass surfaces according to reactions like Diels-Alder cycloaddition reaction [17-19]. With ultra-high surface-area-to-volume ratios and ultrashort diffusion length, the sealed nanochannels provide a remarkable arena for affinity-based recognition events such as immunoassays or DNA analysis. However, in the case of direct bonding at low temperatures, the immobilization of temperature-sensitive biomolecules should be performed after the bonding process to protect from any possible denaturation (e.g. proteins denature at temperatures above 40 °C [20]). The DNA microarray technique has flourished over the past few years since the partial modifications of nanochannels with DNA ligands with functionality and specificity enable more data than single-point experiments [21]. In this occasion, however, the bottleneck lies in the formation of covalent bonds at pre-determinate spots to immobilize different ligands only to portions of the channel, which is difficult to achieve after bonding due to the limited extended-nanospace. In order to solve this technical issue, the room-temperature direct bonding of glass chips to realize partial functionalization of channels prior to bonding offers a considerably attractive solution.

To date, the realization of room-temperature bonding essentially relied on surface modification via dry or wet approaches. Regarding surface dry activation, a wafer-level glass-glass bonding was achieved at room temperature successfully via reactive ion etching (RIE) O_2 plasma followed by N_2 radical microwave (MW) plasma activation in the same chamber (so-called sequential plasma activation) [22]. Similarly, Takeuchi and co-workers obtained a glass-glass interface with a bonding energy of 1.32 J/m^2 by means of Ar ion bombardment under ultrahigh vacuum ($<10^{-5}$ Pa) conditions, cooperating with in-situ AlO film deposition on the glass surfaces [23]. However, owing to the necessity of special activation equipment, the productivity of nanofluidic applications based on the above methods was greatly limited. In contrast, room-temperature bonding based on surface wet chemical cleaning broke the dilemma of special equipment. For instance, glass-glass interfaces could be attained through the room-temperature treatment of sulfuric acid (H_2SO_4) [24], hydrofluoric acid (HF) [25], or hydrogen fluoride steam [26]. Nevertheless, the extensive utilization of dangerous chemicals was not conducive to establishing a toxic-free environment and should be avoided for non-essential societal use. Furthermore, the essence of HF activation lies in the sufficient SiO_2 etching rate (10 nm/min) based on the chemical reaction (SiO_2 +

$4HF \rightarrow SiF_4\uparrow + 2H_2O$), which could destroy the fine nanostructures in the devices [25]. Recently, a water-droplet bonding method was developed to realize room-temperature glass bonding via H_2O as the bonding agent [6]. The pressure endurance of more than 600 kPa within 6 h of bonding was sufficient for cell cultivation, but far from suitable for high-pressure nanofluidic scenarios. Overall, these methods are not cost-effective, nano-structure friendly, or robust enough for the mass production of glass nanofluidics.

Polytetrafluoroethylene (PTFE), also termed Teflon, is generally not suitable as a bonding agent due to its superior chemical inertness under the harshest conditions below 300 °C [27, 28]. Notwithstanding, we proposed a technically convenient PTFE-assisted plasma modification strategy via commercialized reactive ion etching equipment to construct fluorinated glass surfaces for room-temperature (RT, 25 °C) direct bonding in this work. Different from the significant etching effect of HF, the fluorine radicals (F^*) from PTFE pieces were introduced on the glass surface via O_2 plasma sputtering and partially replaced Si-O with Si-F groups within 40 s, which was considered to be friendly to fine nanostructures. The RT bonding mechanisms were analyzed based on X-ray photoelectron spectroscopy (XPS) and chemical affinity results, and the leak-free glass-glass interface with high bonding energy was examined via leakage test under high-pressure nanofluidic conditions (2 MPa). In addition, the light transmittance of the bulk glass substrate and across the bonding interface was also evaluated, demonstrating the capacity for sensing and diagnostics.

2. Experimental section

2.1 PTFE-assisted surface modification process

The fused-silica glass substrates (70 mm × 30 mm × 0.7 mm) without nanochannels were used in this study to investigate the possibility of room-temperature bonding. Firstly, the glass substrates were immersed in piranha solution (H_2SO_4:H_2O_2=3:1) for 8 min to remove the organic contaminants effectively. Subsequently, the contamination-free glass substrates were ultrasonically cleaned with deionized water for 5 min and dried via nitrogen flow. To modify the glass substrates with PTFE, the clean glass substrates were placed into the center of the plasma activation chamber side by side while introducing a square frame-shaped PTFE substrate (5 mm thick, 2.18 g/cm^3) to surround the glass substrates simultaneously, as shown in Fig. 1. The O_2 gas was introduced into the chamber at a pressure of 60 Pa, and the plasma was generated with a discharge power of 200 W at a frequency of 13.56 MHz. Due to the activation and sputtering effect of plasma on glass and PTFE, the glass surfaces can be functionalized via treatment for 40 s, and the F concentrations on the glass surface can be controlled by adjusting the area of the PTFE frame during plasma activation. After the surface activation, two glass substrates were exposed to a storage chamber to achieve subsequent bonding within 30 s, which could control the relative humidity (RH) to terminate the glass surfaces with sufficient H_2O molecules. Owing to the H_2O molecules playing an important role in bridging the microgaps between the surfaces, Fig. S1(a) displays the bonding area ratio as a function of relative humidity. The effective bonding area was estimated by Photoshop software and was compared with the total bonding area of glass-glass chips. It can be noticed that the bonding area ratio exceeded 95% stably when the RH was more than 75%. The lack of H_2O

molecules could barrier establishing hydrogen networks between the surfaces. Herein, the optimal relative humidity of the storage chamber was 75%. When the glass surfaces were brought into contact, slight pressure was applied from one side of the chip with a tweezer to generate a bonding wave. Once the bonding wave started propagating across the interface, there was no requirement for pressure and a completely bonded interface would be obtained spontaneously. To further stabilize the interface, the glass-glass pairs should be stored at room temperature for 48 h, and the bonding strength and feasibility for nanofluidic devices were subsequently further evaluated. Considering the possible condensation reactions at the interface, the bonded samples were all positioned in a ventilated place such as a ventilating cabinet to facilitate the timely release of trace gaseous by-products.

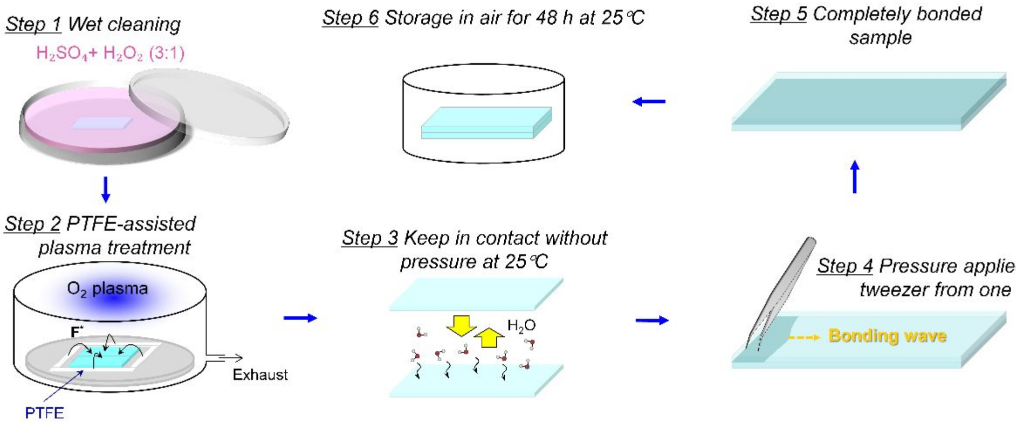

Fig. 1. Schematic drawing of room-temperature bonding of glass chips via fluorinated plasma introduced by PTFE.

2.2 Evaluation of bonding energy

To assess the bonding energy, the crack propagation length was recorded to calculate bonding energy via the crack-opening method [29]. This is the most convenient method to measure the strength of bonded samples. A razor with a thickness of t_b (100 μm in this work) was inserted into the bonding interface. The bonding energy (γ) can be obtained via the following equation:

$$\gamma = \frac{3t_b^2 E t_w^3}{32L^4}$$

where E is Young's modulus for the fused silica substrate (6.6×10^{10} Pa), t_w is the glass substrate thickness (7×10^{-4} m), and L is the crack propagation length.

2.3 Leakage test

Chips with two sets of microchannels bridged with 20 parallel nanochannels were fabricated on glass substrates for leakage test, which is a standard micro/nano hybrid fluidic circuit for liquid manipulation in nanofluidic applications. In this micro/nano hybrid system, the microchannels facilitated the entry and regulation of liquids as well as the external connection on demand, while the nanochannels were employed for subsequent measurement. This nano-in-microfluidic system has distinctive advantages of steady liquid introduction, effective liquid exchange, and prevention of bubbles or dust entering nanochannels. Therefore, the nano-in-microfluidic system is not only applicable for DNA/RNA analysis [21, 30], but also for streaming potential/current measurement [31] or in-situ electrokinetic probing [32] for the investigation of extended-nanospace chemistry, as an electrochemical reactor for enzymatic reaction [33, 34] to enhance reaction rates, and the accurate active regulation of femtoliter-scale fluid flow [35], etc. To be precise, the nanochannels were patterned on one side of the substrate by electron beam lithography, and two sets of microchannels were formed by photolithography on the other substrate, both of which were then subjected to plasma dry etching. Moreover, the inlet/outlet holes at the end of microchannels were also drilled. The patterned glass substrates integrated by the abovementioned PTFE-assisted modification were ready to perform leakage tests. Herein, we designed and developed a two-channel high-pressure liquid introduction system instead of a common air controller to inject sample solution into the micro and nanochannels under a wide pressure range (50 kPa~2 MPa), which will be illustrated in detail later. By pressure switching and blocking one of the inlet holes of a microchannel, the fluorescent sample solution would be pressured into nanochannels and another microchannel. Eventually, the channels filled with sample solution and leakage at the bonding interface could be checked on a nanometer-scale level using fluorescence microscopy. Considering the adsorption of fluorescence dye on the glass walls, sulforhodamine B (10 µmoL/L) was chosen as the fluorescent solution and introduced into the microchannel to avoid interference results and ensure repeatability.

3. Results and Discussion

In order to elucidate the effect of PTFE-assisted modification, the chemical state of glass substrates before and after activations were analyzed by X-ray photoelectron spectroscopy (XPS) first. As displayed in Fig. 2(a), the symmetric peak at 103.9 eV in Si 2p spectra of pristine glass substrates was assigned to the Si-O bonds [36]. When the glass substrate was treated only with O_2 plasma without a PTFE frame, the Si-O peak position shifted to the higher binding energy. This shift can be attributed to the organic contamination desorption on the pristine surface via chemical bonds (e.g. C-Si-O) breakage. After O_2 plasma activation, the contamination decomposed into CO_2 and H_2O, and more Si-O dangling bonds were exposed owing to the reactive oxygen radicals (ROS). Concurrently, Fig. 2(b) shows that there were no F-related signals detected on the O_2 plasma-activated glass surface. However, the F signal emerged on the PTFE-assisted activated surface at 685.2 eV which was attributed to Si-F bonds [37]. Due to the sputtering effect of ions with kinetic energy and the reactivity of ROS generated in O_2 plasma, the C-F bonds of the PTFE were broken through chemical oxidation to form CO, CF_xO_y, and most important fluorine radicals (F^*), as shown in the reaction (1) [28, 38]. The gaseous CO and CF_xO_y could desorb from the PTFE surface, while neutral F^* could diffuse onto the glass surface. These small amounts of reactive F^* would not cause extensive bond breakage but partially broke Si-O bonds to terminate the glass surface with Si-F following exothermic reaction [39]. Given that the essence of PTFE-assisted modification is the introduction of F^*, this functionalization can also be denoted as (O_2 + F^*) plasma activation.

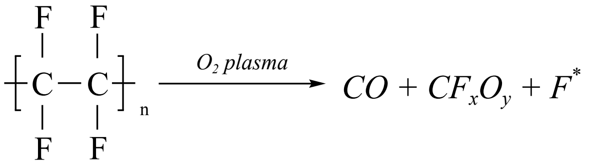

$$\left[-CF_2-CF_2- \right]_n \xrightarrow{O_2\,plasma} CO + CF_xO_y + F^* \qquad (1)$$

In addition, the XPS compositional depth analysis was also carried out using an Ar-ion beam at an incident angle of 35°, as presented in Fig. S2. As the surface was etched, it turns out that the F signal was still detectable down to a depth of ~2 nm, suggesting the formation of fluorinated silicon oxide (SiO_xF_y) on the subsurface. To assess the uniformity of the fluorinated silicon oxide, the relative atomic concentration (atomic percentage, at.%) of F could be quantitatively characterized and calculated via XPS on the different positions of the glass surface, including the corner and center parts. As shown in Fig. S3(a), the fluorine concentrations at five positions of the glass surfaces were analyzed. The relative atomic concentration of fluorine was calculated from the ratio of the fluorine peak areas to the total peak areas in the XPS measurements. It turns out that the concentration of fluorine at the center was slightly lower than at the corners due to the sputtering-like process using peripheral PTFE as the fluorine source, as displayed in Fig. S3(b). The average fluorine concentration (at.%) was 5.522%, demonstrating the formation of a fluorinated oxide layer over the entire 30 mm×70 mm glass surface.

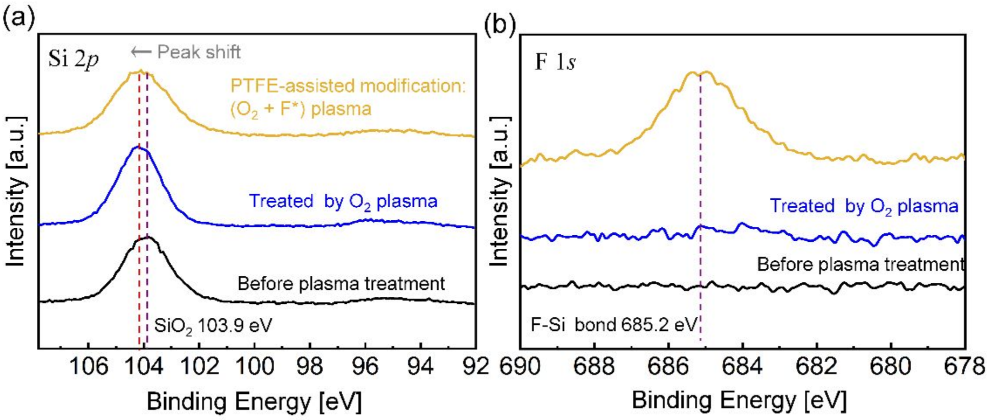

Fig. 2. XPS (a) Si 2p and (b) F 1s core level spectra of glass substrates before and after activations.

Albeit the fluorinated glass surface has been formed via (O_2+F^*) plasma activation due to the assistance of PTFE, the surface morphology is an important factor that represents the real contact area between the surfaces to assess whether bonding can occur at room temperature. Evaluation of surface roughness in terms of root-mean-square (RMS) values and three-dimensional morphology analysis was achieved by atomic force microscopy (AFM). According to the reduced RMS values (<0.15 nm) shown in Fig. 3(a), it is indicated that the glass surface was slightly flattened after O_2 plasma activation due to the desorption of contaminants. Contrastly, the glass surface was roughened with the addition of F^* in O_2 plasma, and the average RMS value increased to 0.2 nm, even exceeding that of the bare glass surface. Since the fluorinate-containing gas plays an important role in the etching of SiO_2 during the semiconductor fabrication in the industry, the slightly rougher glass surface obtained via (O_2+F^*) plasma can be attributed to the etching effect of F^*. Due to the low concentration of F^* radicals, however, the surface morphology has not deteriorated further, which was still smooth enough (<0.5 nm) and conducive to room-temperature bonding. Moreover, AFM 3D images of glass substrates fabricated with nanochannels (100 nm in depth, 2 μm in width) before and after (O_2+F^*) plasma activation were also displayed in Fig. 3 (b) and (c). It can be observed that there is little change in the morphology of the nanochannels after (O_2+F^*) plasma activation, indicating that the low concentration of F^* will not damage the precise nanostructures on the glass substrate. Therefore, due to the cleaning effect of ROS and the etching action of F^*, (O_2+F^*) plasma currently appeared to be a viable candidate for bonding glass substrates with complex nanostructures.

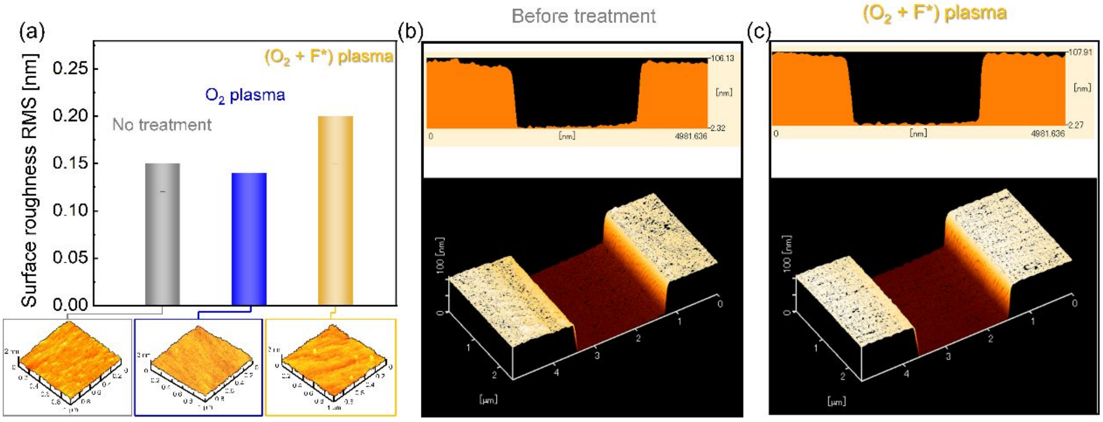

Fig. 3. (a) Surface roughness and topography of glass substrates before and after different activations. AFM images of a shallow nanochannel before and after (O_2+F^*) activation are shown in (b) and (c), respectively.

The Si-F groups have been established on the smooth glass surface, while the resultant surface energy was ought to be further appraised of the correlation between the surface energy and bonding difficulty. According to the Young equation [40], wettability represents the surface energy that can be collected by the water contact angle test. Fig. 4 presents the water contact angle of the glass surface as a function of F concentration on the surface. When the F concentration was reduced to 0 (O_2 plasma activation), water droplets spread rapidly on the surface because of the construction of high-density –OH functional groups, and the final contact angle was stabilized at 3°. With the incorporation of sufficient –OH groups, the bonding wave was prone to propagating across the interface even with slight pressure applied with a tweezer. With the addition of F atoms, the contact angle increased significantly and could reach 51° when the F concentration was 11.2%. The relatively hydrophobic glass surface realized via (O_2 + F^*) plasma was attributed to the electronegativity of F, causing the polar hydrophobicity [41]. However, the room temperature bonding could not be realized with this high concentration, indicating that the excessive F atoms had a detrimental effect on bonding.

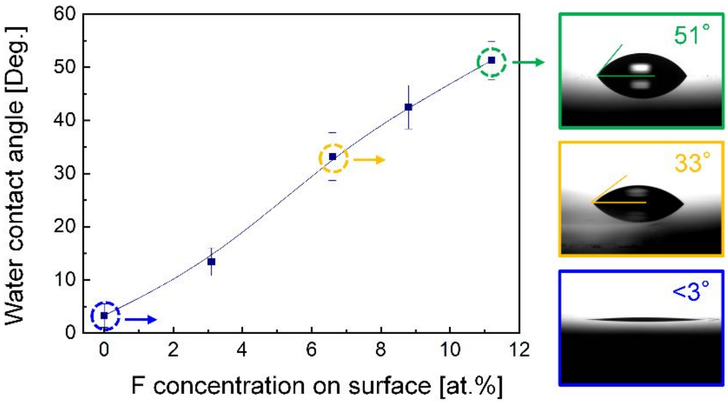

Fig. 4. Hydrophilicity of glass substrates as a function of F concentration on the surface.

Considering the effect of fluorination, it is necessary to optimize the F concentration to achieve optimal bonding energy. Without the plasma treatment, the glass substrates were almost impossible to be bonded, and a fairly weak bonding energy of 0.125 J/m^2 was obtained, as displayed in Fig. 5(a). Once the surfaces were activated by O_2 plasma, the bonding strength was rapidly improved to 0.6 J/m^2 after room temperature storage for 48 h, while it was still not robust enough for nanofluidic applications. Subsequently, optimal F concentration was screened as 5% with the assistance of PTFE, obtaining the maximum bonding energy of 1.534 J/m^2 with a crack opening length of 10.85 mm, as displayed in Fig. 5(b). In addition, the tensile test was also performed for the glass-glass interface with maximum bonding energy. As shown in Fig. 5(c), the room-temperature bonding interface exhibited good bonding strength with maximum values of 11.3 MPa. However, the further introduction of F atoms could degrade the bonding energy, which was in accordance with the contact angle results. Furthermore, the activated surfaces with optimal F concentrations should be bonded without long-term exposure to preserve surface reactivity. Otherwise, the bonding strength and area would inevitably deteriorate. Fig. S4(a) presents the bondability of activated surfaces with different air exposure times before bonding in the atmosphere with RH=75%. Combined with Fig. S4(b), it can be noted that the optimal strength and bonding area could be attained simultaneously via timely bonding. However, one can notice that the bonding strength decreased slightly when the functionalized surfaces were bonded within 0.5 h, but still exceeded 8 MPa. With the prolongation of exposure time, the bonding strength was degraded further, and the obvious unbonded regions with Newton rings were observed, as depicted in Fig. S4(c). Ultimately, the surface became completely inactive after 2.5 hours of exposure. Therefore, a maximum storage time of 0.5 h in an atmosphere of RH = 75% was recommended to ensure the bonding quality. Similarly, Xu et al. [42] introduced F* on glass surfaces via the mixture of O_2/CF_4 plasma to obtain the optimal glass-glass bonding energy (1.12 J/m^2) at room temperature. However, the flow rate of CF_4 should be precisely controlled at 0.5 sccm via accurate gas flow controllers, which was expensive to equip with a commercial plasma chamber. Therefore, it is a more convenient and cost-effective solution to generate F* from PTFE. Moreover, it is reported that the bonding energy of O_2 plasma-activated Si-Si pairs can be saturated via long-term storage like 4000 h [43], indicating the sufficient occurrence of reaction between the hydroxylated interface. Similarly, it can be speculated that the glass-glass interface obtained by O_2 plasma activation can be further strengthened via storage, whereas this duration could be effectively shortened via (O_2+F*) plasma treatment.

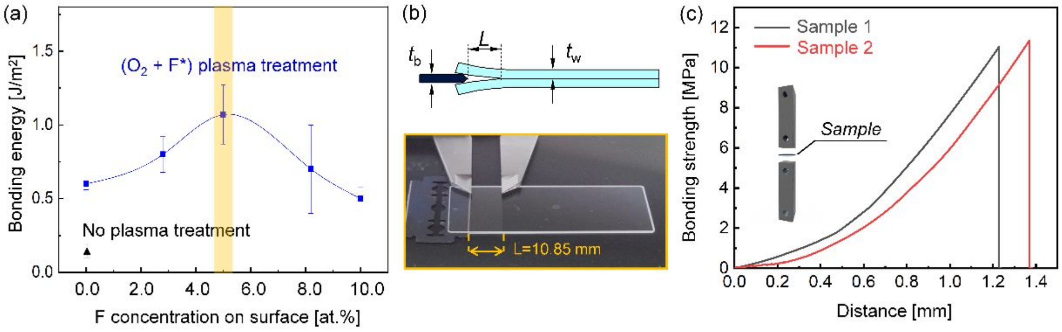

Fig. 5. (a) Evaluation of room-temperature bonding energy with different F concentrations on the surface. The photograph of the crack opening with maximum bonding energy is shown in (b). (c) Tensile strength-distance curve of bonding interface with optimal F concentrations on the surface.

Combining the above results, the mechanism of room-temperature bonding via PTFE-assisted plasma modification can be illustrated, as shown in Fig. 6. When the glass surface was exposed to O_2 plasma, a sufficiently smooth, hydrophilic surface terminated with sufficient –OH groups was achieved. A hydrogen network could be formed between the hydroxylated glass surfaces with the help of water molecules, determining whether bonding can take place [44]. With increasing temperature or prolonged storage, the weak hydrogen bonds could be converted into strong covalent bonds according to the dehydration reaction (2), which is reversible up to 425 ℃ [45]. The more by-product H_2O molecules diffused from the interface, the more Si-O-Si covalent bonds were formed, which is more conducive to the strengthening of the interface. Therefore, the interfacial structure had an important influence on the enhancement of bonding energy.

$$\text{Si-OH} + \text{HO-Si} \rightarrow \text{Si-O-Si} + H_2O \tag{2}$$

Nevertheless, by activating the glass surface with (O_2+F^*) plasma, an outermost surface terminated with Si-OH and Si-F groups and a subsurface structure of SiO_xF_y were obtained. Given the polar hydrophobicity of Si-F groups, the water adsorbed on the plasma-activated surface could be controlled by balancing the amount of –OH and –F groups. Appropriate addition of F could limit the adsorption of H_2O on the surface, whereas the excessive hydrophobic groups on the surface could barrier the bonding at room temperature since the hydrogen network cannot be formed with a small number of water molecules [45]. On the other hand, the SiO_xF_y in the subsurface with adequate thickness played a crucial role in facilitating the diffusion of H_2O like a porous “sponge”. This is because fluorinated silicon oxide has a lower density than SiO_2 due to its large ring structure [46, 47]. Therefore, the establishment of Si-OH and Si-F on the glass surface via PTFE modification restricted the adsorption of water molecules initially. After the two glass surfaces came into contact, a hydrogen network was established and the dehydration reactions (2) and (3) occurred at room temperature. Owing to the smaller volume of HF molecules, the diffusion rate of HF in oxides could be much faster than that of H_2O molecules. Subsequently, the SiO_xF_y with a thickness of 2 nm in the subsurface could facilitate the diffusion or dissolution of H_2O and HF at the interface effectively. Eventually, a robust Si-O-Si covalent network was realized by storage for 48 h in ambient air. In addition, we characterized the room-temperature bonding energy of glass-glass as a function of storage time in ambient air, as shown in Fig. S1(b). One can note that the bonding interface was strengthened significantly and continuously within 24 h. After 24 hours of storage, the interface was shown to be robust enough (>1.0 J/m^2) to withstand the post-bonding process such as dicing [48], illustrating a bonding efficiency comparable to sequential plasma activation (24 h) [22]. Upon the storage duration exceeding 48 h, the maximum bonding energy was obtained, indicating the sufficient occurrence of dehydration reactions.

$$\text{Si-OH} + \text{F-Si} \rightarrow \text{Si-O-Si} + \text{HF} \qquad (3)$$

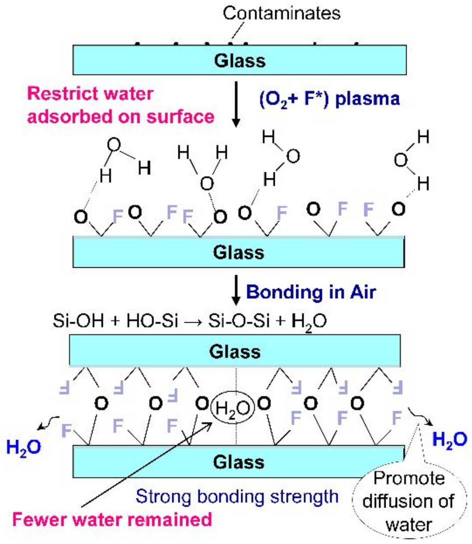

Fig. 6. The mechanism of room-temperature bonding of glass chips via PTFE-assisted modification.

Regarding room-temperature bonded glass substrates, there is an urgent need to confirm whether the glass modified via PTFE met the requirements for nanofluidic devices. Thereby, a leakage test was applied to the glass substrates fabricated with micro and nanochannels. Since the nanofluidic channels usually should be able to withstand high pressures of hundreds of kilopascals, here the fluorescent solution was driven into the channels by a self-designed two-channel high-pressure liquid introduction system to verify the bonding strength, which can provide continuous, precise, and higher pressure (50 kPa~2 MPa) required for common nanofluidic applications. As illustrated in Fig. 7(a), N_2 gas was generated from a gas cylinder and the gas pressure was increased up to a maximum of 4.4 MPa using a compressor. The pressured N_2 gas was divided into two channels and stored in two gas tanks (T_g), and the gas pressure in the T_g could be controlled by the connecting solenoid valves SV_1. Afterward, by opening the solenoid valves SV_2, the sample solution (sulforhodamine B) was pushed from the gas tanks into the connecting liquid tanks (T_L), ready to introduce into the nanofluidic chip fixed on the stainless steel microchip holder. The connections between the T_L and nanofluidic chip were sealed with Teflon O-rings. It is noteworthy that one of the liquid tanks was filled with sample solutions from the gas tank, while another liquid tank was just filled with pressed gas to ensure the diffusion of the solution from one side microchannel to the other via 20 bridging nanochannels. As sulforhodamine B was driven into the nanofluidic chip, the leakage could be observed via fluorescence microscopy when the bonding area was filled with fluorescence solution. Eventually, the fluorescence solution could be collected and recycled to the waste tanks (T_w) via solenoid valves SV_3 to keep the experiment environmentally friendly. The actions of all valves could be controlled through an LCD touch panel.

Based on the abovementioned pressure-driven fluidic control system, Fig. 7(b) shows that sulforhodamine B was introduced into the left side microchannel and center nanochannels (400 nm in width, 200 nm in depth, 700 μm in length), which were sealed by (O_2+F^*) plasma activation at room temperature, and effused from the right side microchannel. Due to the higher Laplace pressure in nanochannels, the leakage could be prone to be observed at the nanochannels and connections of the micro and nanochannels. Fig. 7(b) presents that strong fluorescence was checked in the entire 700-μm long nanochannels with the continuous introduction of sulforhodamine B at a pressure of 2 MPa, whereas no fluorescence was observed at the bonding interface between the nanochannels, revealing the defect-free interface and sufficient bonding strength. Moreover, as displayed in Fig. 7(c), the enlarged fluorescence image illustrated that the hermetical seal was realized at the connection of the right microchannel and nanochannels, which suggested the successful introduction of the solution into the microchannel via bridging nanochannels without leakage. The leak-free glass-glass interface verified the capability of nanofluidic devices assembled via (O_2+F^*) plasma to withstand high pressure. In contrast, the fluorescent signal was detected at the connection of the microchannel and nanochannels formed via O_2 plasma activation even at a pressure of 50 kPa, indicating the risk of substrate separation under common nanofluidic conditions. Therefore, the stable and robust glass-glass interface fabricated via PTFE-assisted plasma modification demonstrated the broad prospects spanning sensing, medical diagnostic, high-pressure nano chromatography, etc.

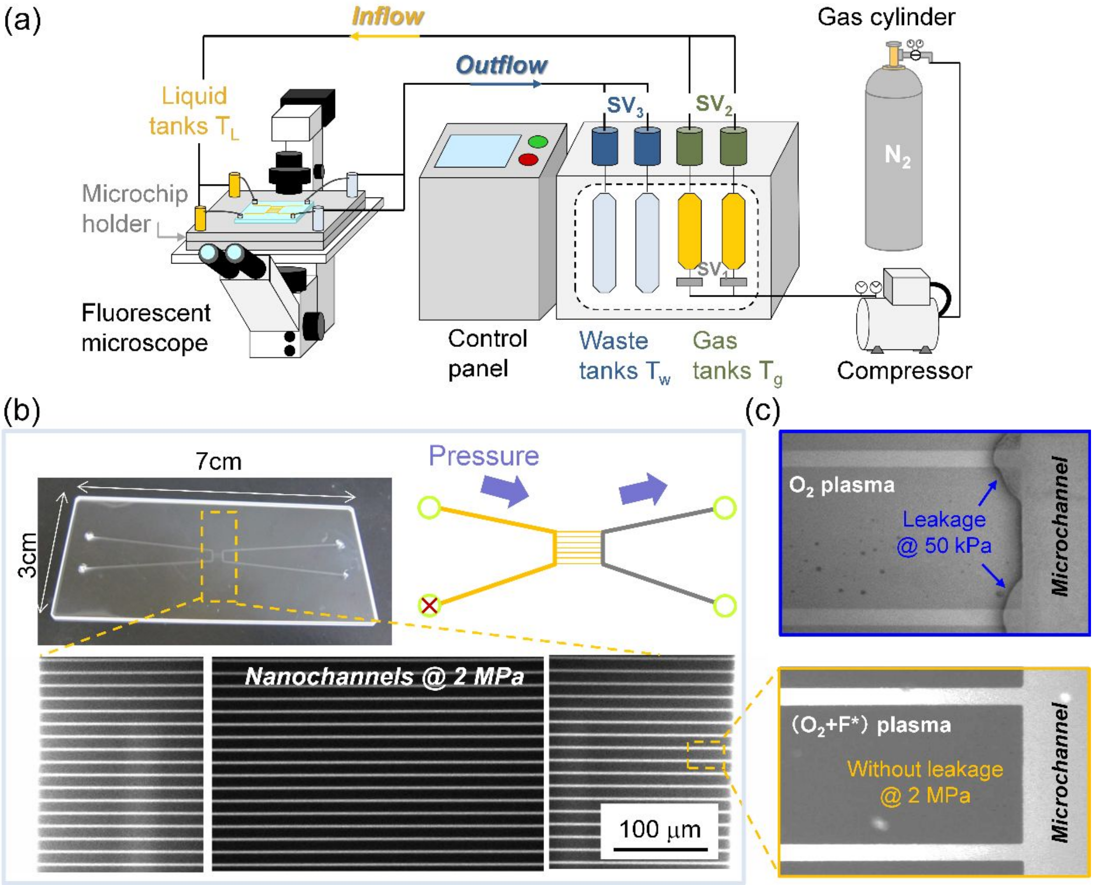

Fig.7. (a) Schematic illustration of high-pressure liquid introduction system for the measurement of nanofluidic leakage. (b) The photograph of bonded glass chips with micro and nanochannels and the fluorescence pictures of nanochannels with the introduction of sulforhodamine B solution. (c) The fluorescence image of the connection of microchannel and nanochannels with different activations.

In addition, the direct transmittance of bulk substrates and bonded glass pairs was analyzed by UV-Vis spectrophotometer in the wavelength range of 200 nm~800 nm. As presented in Fig. 8, the transmittance of bulk glass substrate exceeded 93% in the range of 400 nm to 800 nm, determining the extraordinary optical property of glass substrate as a nanofluidic platform. However, the optical transmittance was reduced by less than 1% for the glass pairs bonded at room temperature via (O_2+F*) plasma, exhibiting relatively high transparency which was close to the bulk glass substrate.

Given the light absorption by the glass itself, it can be concluded that not only there was no defect at the bonding interface, but also the fluorinated SiO_xF_y layer had little effect on the decrease in optical transmittance. Thus, the defect-free bonded glass pairs activated by (O_2+F^*) plasma demonstrated the potential for future high-speed, high-sensitive, and high-resolution optical detection or liquid sensing.

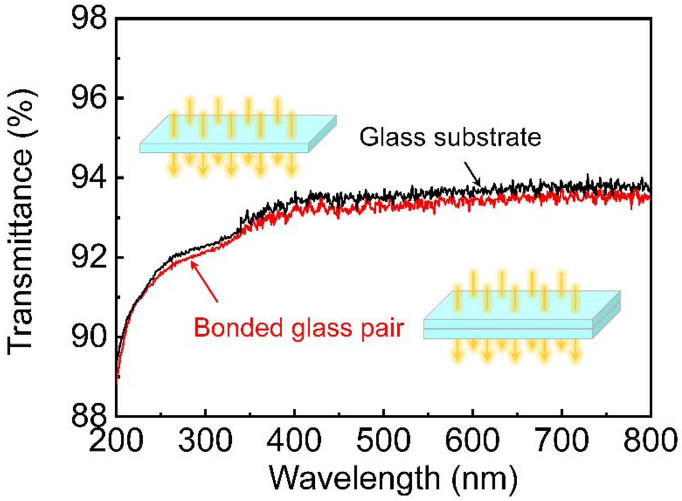

Fig. 8. UV-Vis transmission spectra of the bulk glass (700 μm thick) and the glass/glass bonded pair (1400 μm thick in total).

4. Conclusion

In summary, we developed a strong and nano-structure friendly PTFE-assisted plasma modification strategy for glass-glass bonding at room temperature. Because of the cleaning effect, sputtering effect, and chemical reactivity of O_2 plasma, the fluorine radicals (F^*) were generated from the PTFE in the commercialized reactive ion etching plasma chamber, and the glass surface was flattened and functionalized effectively within 40 s. Although the etching effect of fluorinate-containing gas on SiO_2 was extensively proved, the addition of trace F^* could obtain the smooth glass surface and maintain the profile of precise nanochannels. Without the requirement for immersion of dangerous chemicals such as HF, a Si-OH and Si-F terminated glass surface with fluorinated silica oxide in the subsurface was obtained via the (O_2+F^*) plasma treatment, and this fluorinated SiO_xF_y layer had little effect on the light transmittance. By controlling the F concentration on the surface, the maximum bonding energy of 1.534 J/m^2 was achieved after room-temperature storage for 48 h, which was almost three times stronger than the interface realized by only O_2 plasma activation. Moreover, the capability of this PTFE-assisted plasma modification strategy for nanofluidic devices was verified, and a leak-free glass-glass interface with high-pressure resistance (2 MPa) would exhibit great potential for applications immobilized with temperature-sensitive functional components.

Supplementary Information

The characterization of bonding efficiency with different relative humidity, and room temperature bonding energy of glass-glass as a function of storage time in ambient air. The XPS compositional depth analysis of glass surface activated via (O_2+F^*) plasma. Schematic of five positions on the fused-silica glass surface for the XPS measurements and the atomic concentrations (at.%) of fluorine at the corresponding positions after (O_2+F*) plasma treatment for 40 s. The evaluation of bondability of (O_2+F^*) plasma activated surfaces with different air exposure times before bonding at RH=75% in the atmosphere.

Conflicts of interest

There are no conflicts to declare.

Acknowledgments

This work was financially supported by the National Natural Science Foundation of China (Grant Nos. 51975151 and 92164105), the Heilongjiang Provincial Natural Science Foundation of China under grant LH2019E041, and the Heilongjiang Touyan Innovation Team Program (HITTY-20190013). The authors also acknowledge financial support from the Core Research for Evolutional Science and Technology (CREST) program of the Japan Science and Technology (JST) *via* grant no. JPMJCR14G1.

References

1 D. R. Reyes, D. Iossifidis, P. Auroux and A. Manz, 2002, **74**, 2623–2636.

2 D. Najjar, J. Rainbow, S. Sharma Timilsina, P. Jolly, H. de Puig, M. Yafia, N. Durr, H. Sallum, G. Alter, J. Z. Li, X. G. Yu, D. R. Walt, J. A. Paradiso, P. Estrela, J. J. Collins and D. E. Ingber, *Nat. Biomed. Eng.*, 2022, **6**, 968–978.

3 M. Yafia, O. Ymbern, A. O. Olanrewaju, A. Parandakh, A. Sohrabi Kashani, J. Renault, Z. Jin, G. Kim, A. Ng and D. Juncker, *Nature*, 2022, **605**, 464–469.

4 H. Hisamoto, Y. Shimizu, K. Uchiyama, M. Tokeshi, Y. Kikutani, A. Hibara and T. Kitamori, *Anal. Chem.*, 2003, **75**, 350–354.

5 H. Hisamoto, T. Saito, M. Tokeshi, A. Hibara and T. Kitamori, *Chem. Commun.*, 2001, **1**, 2662–2663.

6 S. I. Funano, N. Ota and Y. Tanaka, *Lab Chip*, 2021, **21**, 2244–2254.

7 Y. Xu, C. Wang, Y. Dong, L. Li, K. Jang, K. Mawatari, T. Suga and T. Kitamori, *Anal. Bioanal. Chem.*, 2012, **402**, 1011–1018.

8 D. I. Rozkiewicz, B. J. Ravoo and D. N. Reinhoudt, *Supramol. Chem. Org. Hybrid Mater.*, 2010, 433–466.

9 Y. Ding, S. Garland, M. Howland, A. Revzin and T. Pan, *Adv. Mater.*, 2011, **23**, 5551–5556.

10 B. Samel, M. K. Chowdhury and G. Stemme, *J. Micromechanics Microengineering*, 2007, **17**, 1710–1714.

11 L. Yu, F. E. H. Tay, G. Xu, B. Chen, M. Avram and C. Iliescu, *J. Phys. Conf. Ser.*, 2006, **34**, 776–781.

12 X. Zhou, S. Virasawmy and C. Quan, *Microsyst. Technol.*, 2009, **15**, 573–580.

13 J. Q. Lu, J. J. McMahon and R. J. Gutmann, *Mater. Res. Soc. Symp. Proc.*, 2009, **1112**, 69–80.

14 N. Y. Lee and B. H. Chung, *Langmuir*, 2009, **25**, 3861–3866.

15 V. Sunkara and Y. K. Cho, *ACS Appl. Mater. Interfaces*, 2012, **4**, 6537–6544.

16 J. Xu, C. Wang, S. Zhou, R. Zhang and Y. Tian, *Ceram. Int.*, 2019, **45**, 16670–16675.

17 M. Zhang, J. Zhao and L. Gao, *Sensors Actuators, A Phys.*, 2008, **141**, 213–216.

18 L. Tang and N. Y. Lee, *Lab Chip*, 2010, **10**, 1274–1280.

19 J. Bart, R. Tiggelaar, M. Yang, S. Schlautmann, H. Zuilhof and H. Gardeniers, *Lab Chip*, 2009, **9**, 3481–3488.

20 M. Iwakura, D. Nakamura, T. Takenawa and Y. Mitsuishi, *Protein Eng.*, 2001, **14**, 583–589.

21 B. Renberg, K. Sato, K. Mawatari, N. Idota, T. Tsukahara and T. Kitamori, *Lab Chip*, 2009, **9**, 1517–1523.

22 M. M. R. Howlader, S. Suehara and T. Suga, *Sensors Actuators, A Phys.*, 2006, **127**, 31–36.

23 K. Takeuchi, F. Mu, Y. Matsumoto and T. Suga, *Adv. Mater. Interfaces*, 2021, **8**, 1–8.

24 Z. J. Jia, Q. Fang and Z. L. Fang, *Anal. Chem.*, 2004, **76**, 5597–5602.

25 H. Nakanishi, T. Nishimoto, M. Kanai, T. Saitoh, R. Nakamura, T. Yoshida and S. Shoji, *Sensors Actuators, A Phys.*, 2000, **83**, 136–141.

26 L. Chen, G. Luo, K. Liu, J. Ma, B. Yao, Y. Yan and Y. Wang, *Sensors Actuators, B Chem.*, 2006, **119**, 335–344.

27 Y. Wang, Y. Xu, S. Dong, P. Wang, W. Chen, Z. Lu, D. Ye, B. Pan, D. Wu, C. D. Vecitis and G. Gao, *Nat. Commun.*, 2021, **12**, 1–8.

28 G. Primc, *Polymers (Basel).*, 2020, **12**, 1–7.

29 W. P. Maszara, G. Goetz, A. Caviglia and J. B. McKitterick, *J. Appl. Phys.*, 1988, **64**, 4943–4950.

30 F. Persson, J. Fritzsche, K. U. Mir, M. Modesti, F. Westerlund and J. O. Tegenfeldt, *Nano Lett.*, 2012, **12**, 2260-2265.

31 K. Morikawa, K. Mawatari, M. Kato, T. Tsukahara and T. Kitamori, *Lab Chip*, 2010, **10**, 871–875.

32 Y. Xu and B. Xu, *Small*, 2015, **11**, 6165–6171.

33 T. Tsukahara, K. Mawatari, A. Hibara and T. Kitamori, *Anal. Bioanal. Chem.*, 2008, **391**, 2745–2752.

34 W. Xu, E. Foster, C. Ma and P. W. Bohn, *Microfluid. Nanofluidics*, 2015, **19**,

1181–1189.

35 Y. Xu, M. Shinomiya and A. Harada, *Adv. Mater.*, 2016, **28**, 2209–2216.

36 A. Kaur, P. Chahal and T. Hogan, *IEEE Electron Device Lett.*, 2016, **37**, 142–145.

37 C. Wang and T. Suga, *ECS J. Solid State Sci. Technol.*, 2016, **5**, P393–P395.

38 J. A. Colony and E. L. Sanford, *Nasa Tm/100681*, 1987, 10.

39 D. J. Oostra, *J. Vac. Sci. Technol. B Microelectron. Nanom. Struct.*, 1986, **4**, 1278.

40 M. A. Miranda, A. Ghosh, G. Mahmodi, S. Xie, M. Shaw, S. Kim, M. J. Krzmarzick, D. J. Lampert and C. P. Aichele, 2022, 1–17.

41 S. Roy, B. Biswas, N. Ghosh, P. C. Singh and J. A. Mondal, *J. Phys. Chem. C*, 2019, **123**, 27012–27019.

42 T. Plach, K. Hingerl, S. Tollabimazraehno, G. Hesser, V. Dragoi and M. Wimplinger, *J. Appl. Phys.*, , DOI:10.1063/1.4794319.

43 Q. Y. Tong and U. M. Gösele, *Adv. Mater.*, 1999, **11**, 1409–1425.

44 Q. Y. Tong and U. M. Gösele, *Adv. Mater.*, 1999, **11**, 1409–1425.

45 Q. Y. Tong and U. M. Gösele, *Semiconductor Wafer Bonding: Science and Technology*, Wiley, New York (1999).

46 A. Kazor, C. Jeynes and I. W. Boyd, *Appl. Phys. Lett.*, 1994, **65**, 1572–1574.

47 V. Pankov, J. C. Alonso and A. Ortiz, *J. Appl. Phys.*, 1999, **86**, 275–280.

48 H. Takagi, Y. Kurashima, A. Takamizawa, T. Ikegami and S. Yanagimachi, *Jpn. J. Appl. Phys.*, 2017, **57**, 02BA04.